Journal of King Saud University – Science (2018) 30, 337–351

King Saud University
Journal of King Saud University – Science
www.ksu.edu.sa
www.sciencedirect.com

Synthesis and thermo-chemical stability properties of 4,4′,4″-((1,3,5-triazine-2,4,6-triyl)tris (oxy))trianiline/4,4′-(4,4′-Isopropylidene-diphenoxy)bis(phthalic anhydride) hyperbranched polyimide

Muhammad Bisyrul Hafi Othman [a,b], Zulkifli Ahmad [a], Hasnah Osman [b], Muhammad Safwan Mohaiyiddin [c], Hazizan Md Akil [a,*]

[a] *School of Materials and Mineral Resources Engineering, Engineering Campus, Universiti Sains Malaysia, Seri Ampangan, 14300 Nibong Tebal, Pulau Pinang, Malaysia*
[b] *School of Chemical Science, Universiti Sains Malaysia, 18000 Minden, Pulau Pinang, Malaysia*
[c] *School of Materials Engineering, Universiti Malaysia Perlis, 02600 Arau, Perlis, Malaysia*

Received 21 November 2016; accepted 20 December 2016
Available online 11 January 2017

KEYWORDS

Hyperbranched polyimide (HPI);
S-triazine ring;
Degree of imidization;
Thermally stable;
Highly chemical stable

Abstract In this paper, a highly chemical stable 4,4′,4″-((1,3,5-triazine-2,4,6-triyl)tris(oxy))triani line (TTA) was successfully synthesized with 4,4′-(4,4′-Isopropylidene-diphenoxy)bis(phthalic anhydride) (BPADA) using direct nucleophilic addition in Dimethylformamide (DMF). The resulting Hyperbranched Polyimide (HPI) was characterized by means of conventional methods such as Fourier transform infra-red (FT-IR) and proton nuclear magnetic resonance (^{1}H NMR) spectroscopy, gel permeation chromatography (GPC), solubility tests, Field Emission Scanning Electron Microscopy (FESEM), Electron Diffraction X-ray analysis (EDX), Vickers hardness test, thermogravimetric analysis (TG), differential scanning calorimetry (DSC), and thermal conductivity. High molecular weight was obtained by extending the reaction time for 2 h. The TTA/BPADA HPI demonstrated a high chemical stability and could be readily used in the precursor state. The thermal curing led to an increase of the imidization degree and greatly improved the thermal stability (*Tg* above 200 °C, maximum mass loss > 500 °C and char yield > 55%), due to an increasing

* Corresponding author. Fax: +60 4 594 1011.
E-mail address: hazizan@usm.my (H.M. Akil).
Peer review under responsibility of King Saud University.

Production and hosting by Elsevier

http://dx.doi.org/10.1016/j.jksus.2016.12.003

chain packing density). Therefore, it is believed that this incorporated HPI structure containing s-triazine moieties in a polyimide system shows potential as a new high performance and highly functional material.

1. Introduction

Nowadays, different aspects of the synthesis of new polyimide (PI) structures as well as their properties are being explored. Among these are halogenated polyimides (Ando, 2004; Choi et al., 2009), porous polyimides (Othman et al., 2011), polyimides containing flexible linkages (Othman et al., 2015a), composite polyimides (Cornelius and Marand, 2002; Zhang and Srinivasan, 2007), and hyperbranched polyimides (HPI) (Othman et al., 2015c; Suzuki et al., 2004). As an alternative to the branches of active researches and prospects, HPIs based on S-triazine moieties are known to impart good chemical and thermal properties by counterbalancing the optoelectronic properties and maintaining the thermal stability of the HPI material (Dallas et al., 2008). Although most direct polymerizations in HPI systems involve the *A*2 + *B*3 (*dianhydride + triamine*) approach and are comprised of S-triazine moieties that lead to gelation, this phenomenon can be avoided by following stringent polymerization conditions, and the HPIs can even be prepared at high conversions.

Mahapatra and Karak (2007) synthesised two aromatic HPIs with s-triazine rings using this approach, which resulted in high yields (82–90%) and flame-retardant characteriztics (no weight loss was observed below 250 °C under a nitrogen atmosphere and a glass-transition temperature within the range of 230–240 °C). This encouraged the preparation of HPI based on 1,3,5-Triazine-2,4,6-triamine (Melamine)/4,4′-(4,4′-Isopropylidene-diphenoxy)bis(phthalic anhydride) (BPDA), and the resulting material was thermally stable up to 450 °C with a *Tg* of around 196 °C (Othman et al., 2015c), while the thermal degradation behavior was distinguished by the different terminal groups (Othman et al., 2015b). Sojitra et al. (2010) reported the successful synthesis of HPI with favorable properties of higher thermal stability along with good processability. They believed that the resulting characteriztics were due to the choice of the s-triazine nucleus, where the high thermal stability was derived from its molecular symmetry and aromaticity.

However, the study by Sojitra et al. (2010) was strictly limited to the properties that resulted from the symmetric monomers. Further modifications to the chemical structure of the HPI contained s-triazine moiety by the introduction of phenoxy linkage to effects on the flexibility of the S-triazine moieties into the HPI backbone, have yet to be investigated. There still remains a lot of room for improvement, especially with regard to the balancing of HPI properties in their extended chemical structures and in their fully imidized forms, for example, to optimize between of the glass transition temperature (T_g) and/or the flexibility and/or the transparency of the films. The challenge being faced by optoelectronic technology is to maintain an optimized value between both the thermal and optical properties of HPIs (Mittal, 2007; Sroog, 1976).

In the current research, a series of new aromatic HPIs containing s-triazine rings were synthesized from *A*3 4,4′,4″-((1,3,5-triazine-2,4,6-triyl)tris(oxy))trianiline (TTA; 98%) and *B*2 4,4′-(4,4′-Isopropylidene-diphenoxy)bis(phthalic anhydride) (BPADA; 98%) and characterized by Fourier transform infra-red (FT-IR), proton nuclear magnetic resonance (1H-NMR) spectroscopy, and gel permeation chromatography (GPC). The influence of the reaction time and the degree of imidization during the thermal curing was investigated by solubility tests, Field Emission Scanning Electron Microscopy (FESEM), Electron Diffraction X-ray analysis (EDX), Vickers hardness test, thermogravimetric analysis (TG), differential scanning calorimetry (DSC) and thermal conductivity.

2. Experimental design

2.1. Materials

Bide Pharmatech Ltd, China, provided 4,4′,4″-((1,3,5-triazine-2,4,6-triyl)tris(oxy))trianiline (TTA; 98%), while 4,4′-(4,4′-Isopropylidenediphenoxy)bis(phthalic anhydride) (BPADA; 98%) was purchased from Aldrich, both were used as received without further purification. Merck was the supplier for Dimethylformamide, (DMF; 99%) and being distilled over calcium hydride and a N_2 flow to remove traces of water before utilisation.

2.2. Synthesis of 4,4′,4″-((1,3,5-triazine-2,4,6-triyl)tris(oxy))trianiline /4, 4′-(4, 4′-Isopropylidene-diphenoxy)bis(phthalic anhydride (TTA/BPADA) HPI

The reactor was purged with N_2 for 5 min before the DMF solvent was poured into a reaction flask. The stirrer was switched on and was continuously purged with N_2. Then, TTA monomer was added into the reactor and stirred at 450 rpm until a homogeneous yellowish brown solution was formed. Then, the BPADA was added, and the mixture was stirred vigorously under a N_2 flow. At certain intervals the reaction mixture was taken out from the reaction flask for its molecular weight inspection. Finally, the samples were pre-baked at 90 °C for 12 h and hard baked before being cooled to room temperature. A summary of the controlled parameters for all the prepared samples is given in Table 1.

2.3. Characterization of TTA/BPADA HPI series

The chemical structure were confirmed by using Fourier transform infra-red (FT-IR) spectra (Spectrum GX Perkin Elmer) and proton nuclear magnetic resonance (^{1}H-NMR) spectra (Bruker 500 Ultra Shield TM Model: 400 MHz). A gel permeation chromatography (GPC) analysis was carried out with the Agilent GPC model 1200 Infinity equipment according to

Table 1 Summary of controlled parameters.

TTA (A3) *mol* (*mass, g*)	BPADA (B2) *mol* (*mass, g*)	DMF *mL*	Time[a] *Min*	Temperature[b] °C	Sample
0.01 (3.99)	0.015 (7.80)	150	15	200	TB015M
0.01 (3.99)	0.015 (7.80)	150	30	200	TB030M
0.01 (3.99)	0.015 (7.80)	150	60	200	TB060M
0.01 (3.99)	0.015 (7.80)	150	120	200	TB120M
0.01 (3.99)	0.015 (7.80)	150	240	200	TB240M
0.01 (3.99)	0.015 (7.80)	150	480	200	TB480M
0.01 (3.99)	0.015 (7.80)	150	480	–[c]	TBT000
0.01 (3.99)	0.015 (7.80)	150	480	120	TBT120
0.01 (3.99)	0.015 (7.80)	150	480	150	TBT150
0.01 (3.99)	0.015 (7.80)	150	480	180	TBT180
0.01 (3.99)	0.015 (7.80)	150	480	200	TBT200
0.01 (3.99)	0.015 (7.80)	150	480	220	TBT220

[a] The reaction time that has been done.
[b] The curing temperature of the sample.
[c] The samples do not undergo a curing process.

polystyrene standards. The solubility was determined by dissolving 0.1 g of the polymer in 10 mL of solvents. The Vickers hardness numbers (VHN) were obtained using a Shimadzu micro-hardness tester Type-M. A scanning electron microscopic- electron diffraction X-ray analyser (SEM-EDX) was performed on a Zeiss SupraTM 35VP at a magnification of 5000X with a gold palladium film as a coating substrate. Thermal analysis were conducted in N_2 atmosphere at a heating rate 10 °C min^{-1} using thermogravimetric analysis (Pyris 6 Thermo Gravimetric Analyser Perkin Elmer instrument: from 50 to 800 °C), and the glass transition temperature (DSC-6 Perkin Elmer Analyser: from 100 °C to 300 °C). The thermal conductivity was determined by using a Hot Disk Thermal Constant Analyser Model TPS 2500S.

3. Results and discussion

3.1. Synthesis consideration

TTA has excellent solubility in DMF compared to other solvents like DMAc, THF, DMSO, NMP, and DMPU. TTA was diluted in DMF prior to adding to the BPADA to prevent competition between the nucleophilicity of the existing water against the BPADA and to protect the dianiline against electrophiles (Harris, 1990), as well as to promote the nucleophilicity and propagation of the TTA, and to initiate attacks against the carbonyl carbon in BPADA. The concentration of the reaction medium was carefully set at $\geqslant$0.1 g/mL to avoid the formation of premature gels at a certain critical point of the solvent and to obtain a high molecular weight with a narrow molecular weight distribution. Since the formation of the polyimide precursor is exothermic, it is also important to note that equilibrium is favored at lower temperatures (Harris, 1990). At high temperatures, the heat energy will cause the initiators to start propagation, an increasing the number of chains and making the reaction medium more viscous as a result of the gel effect. This limits the chain mobility and reduces the propagation stage to extend the chain length, and resulting in low molecular weight and affecting the thermal properties of the HPI. The reactor was equilibrated in a water flow to maintain a temperature of 25 °C. In addition, the imidization at ambient temperatures may result in the formation of water as a by-product. This competition between the dianhydride and water often takes place during propagation reactions and results in the dianhydride being removed from the equilibrium and upsetting the monomer stoichiometry (Harris, 1990; Mittal, 1984). In order to prevent side reactions caused by water, nitrogen gas should be bubbled through the system during the synthesis. The schematic diagram of the route for the synthesis of TTA/BPADA HPI is shown in Fig. 1.

The equilibrium between the primary and secondary amines was established through a rapid proton exchange. After the breakage of the cyclic anhydride bond, the linear amide-acid finally yielded and released the central oxygen of the cyclic intermediate, thereby resulting in a carboxylate leaving the group and being deactivated through hydrogen bonding with a basic solvent. In this work, the TTA/BPADA HPI was obtained without end capping prior to the critical point of gelation by the slow addition of monomers or without using special catalysts and condensation agents. The polymerization was completed by bulking and was stopped before the formation of gel could occur. Finally, the reaction time was considered to have had an important effect on the molecular weight, where an extension in the reaction time resulted in an increase in the propagation period, further driving up the molecular weight (Mittal, 1984, 2009). Therefore, the progress of the reaction was monitored by changes to the molecular weight across time.

Through the GPC analysis, the molecules were sorted by size, with the largest eluting first and the smallest last, and information for the polydispersity index (PDI) was determined. In this work, the GPC micrographs for all the synthesised HPIs showed the dependence of the reaction time on the MWD and PDI (Mw/Mn), and this relationship is summarized in Fig. 2. In this work, the GPC micrographs showed that there was an increase in the molecular weight when the reaction time was extended, and that a high average molar mass (Mn) was achieved after 240 min of reaction. This proved that by extending the reaction time, the propagation period was increased, which drove up the molecular weight. The TTA/BPADA HPI demonstrated a high average molar mass (Mw)

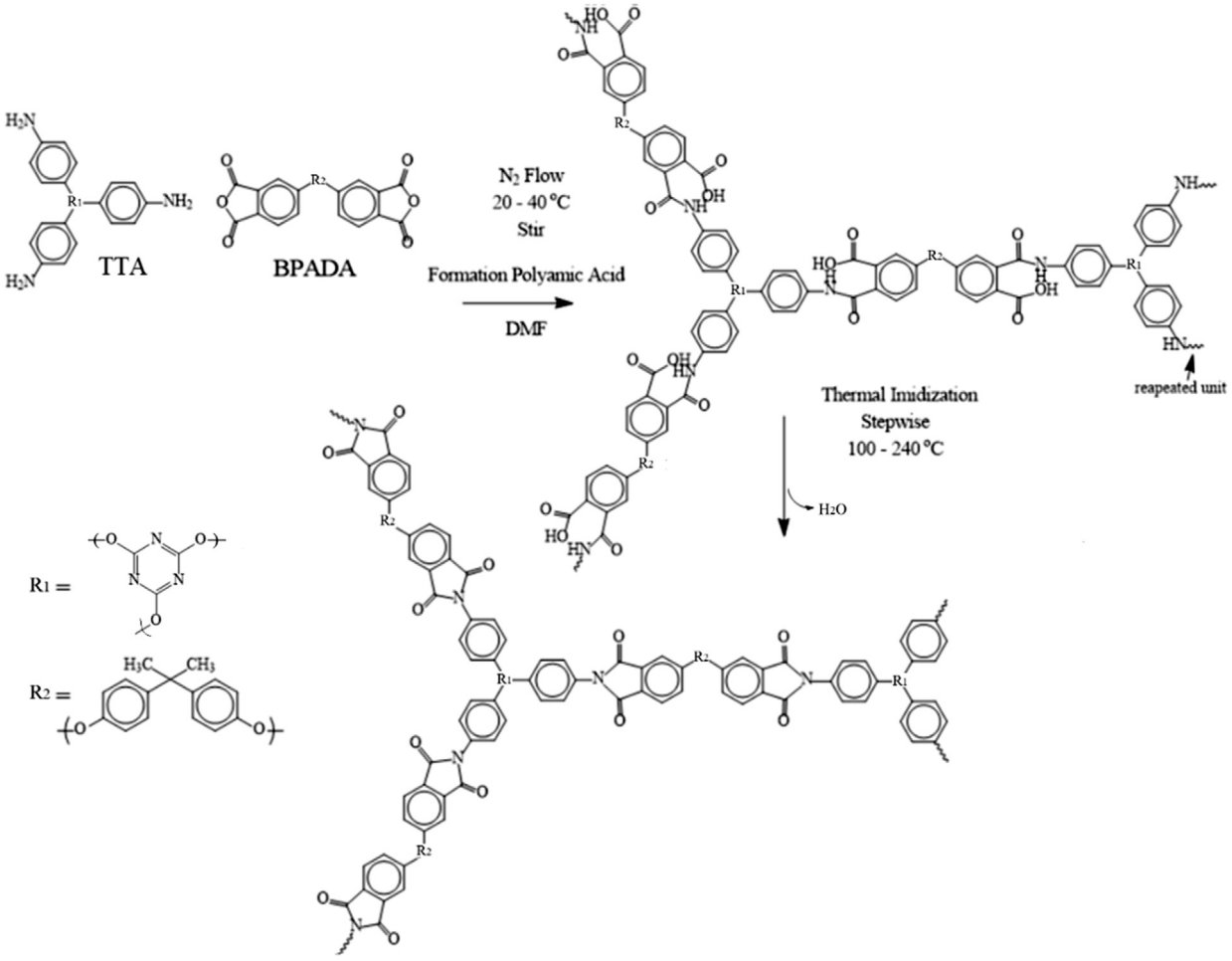

Figure 1 Schematic diagram of the route for the synthesis of TTA/BPADA HPI.

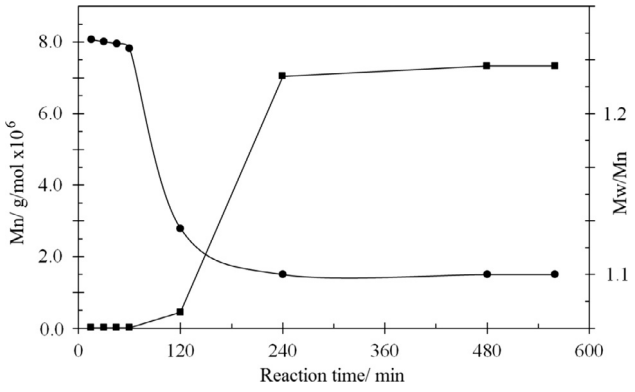

Figure 2 Molecular weight distribution according to reaction time.

of around 700,000, while the PD was 1.00, which implied a narrow MWD.

It was found that this value improved the s-triazine HPI derivatives which had been synthesised by Sojitra et al. (2010) (Mw between 44,000 and 54,000; PD within the range of 1.2–1.9), Jabbari and Nozari (1999) (Mw between 15,000 and 25,000; PD within the range of 1.28–1.40), and Othman et al. (2015c) (Mw between 21,000 and 23,000; PD of 1.20). This was due to the difference in the synthetic route, the monomer reactivity, and the chemical structure that had been utilized. For example, in this case, the TTA was more reactive than cyanuric chloride (Sojitra et al., 2010) and melamine (Othman et al., 2015c). The molecular size and degree of polymerization of a HPI are highly dependent on the effectiveness of the conversion of the monomers to form a polymer chain, which means that a higher molecular weight makes it more viscous, while a more flexible structure (TTA) is better than a rigid structure unfunctionalized s-triazine (Melamine) in order to counter the steric effect during polymerization.

3.2. Structure confirmation

3.2.1. Proton nuclear magnetic resonance

The final structure of the TTA/BPADA HPI was further investigated by means of the solid state ^{1}H-NMR as shown in Fig. 3.

In general, the signals (7.0–8.0 ppm) were assigned to ^{1}Ha, ^{1}Hb, ^{1}Hc, ^{1}Hd, ^{1}He, ^{1}Hf, and ^{1}Hg in reference to the protons of the BPADA aromatic unit with *para*-substitution, where the peaks were separated due to the effects of the protons on the neighboring carbons. At the same time, the signals ^{1}Hh, ^{1}Hi, ^{1}Hj and ^{1}Hk indicated the aromatic amine (~6.90 ppm) and methyl substitution (1.72 ppm) functional group. The ^{1}Ha,

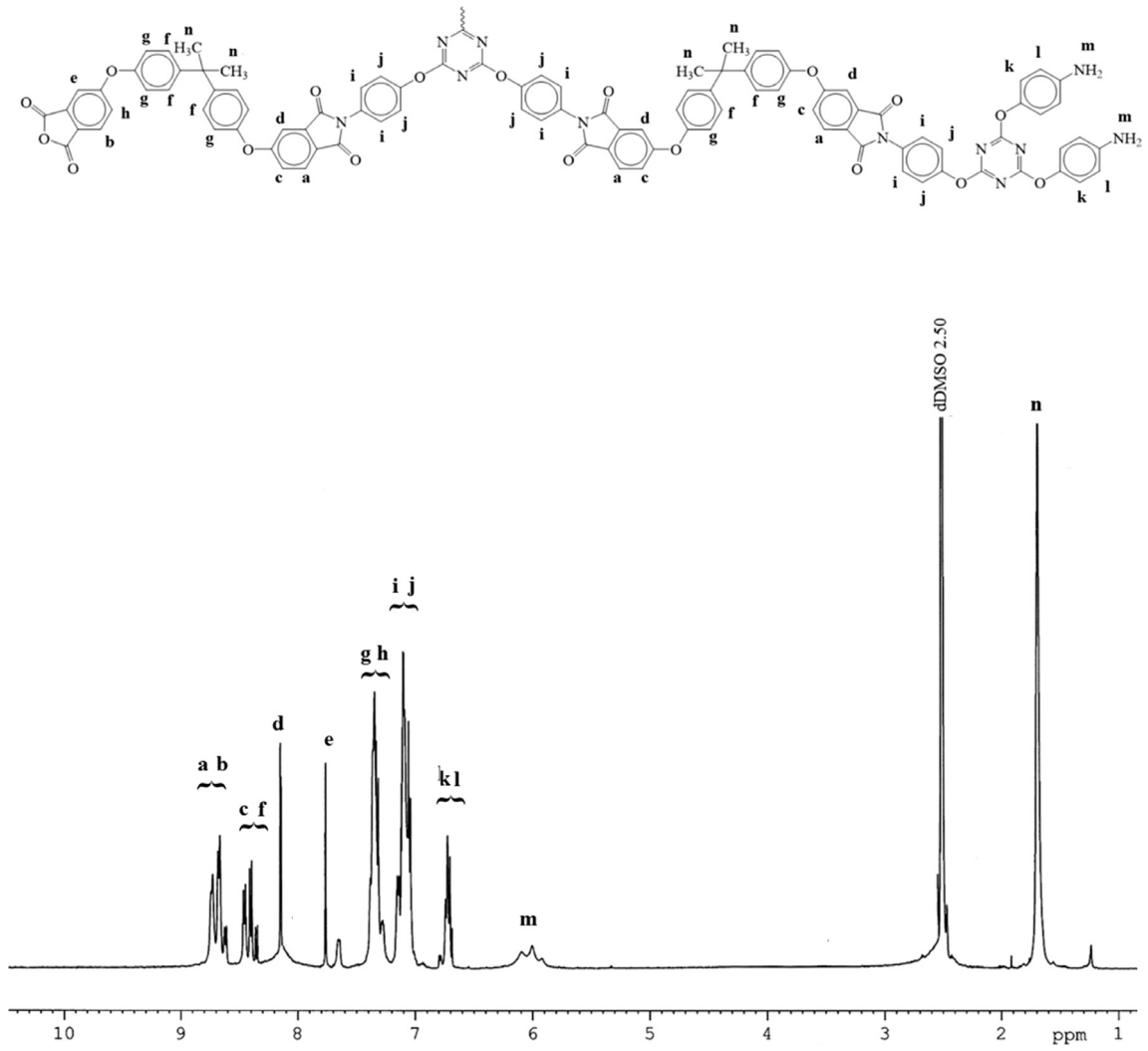

Figure 3 Chemical structure of TTA/BPADA HPI and solid state 1H NMR (400 MHz) spectra.

^{1}Hb, ^{1}Hc, ^{1}Hd, ^{1}He, ^{1}Hf, and ^{1}Hg signals were differentiated by their terminal functional group, which was either amine or anhydride terminated, or both. However, the exact signals for ^{1}Hc, ^{1}Hd, ^{1}He, ^{1}Hf, and ^{1}Hg were difficult to predict due to the cross-linked polymeric material. Although they had similar structures, the environment might have been different and the assigned signals may have been in the given range.

3.2.2. *Fourier transform infrared spectroscopy*

Fig. 4 presents the FT-IR spectra of the TTA/BPADA HPI precursor that was formed through addition polymerization and the TTA/BPADA HPI that was formed through thermal imidization corresponding to a wave number of 4000–550 cm^{-1}. The characteriztics of the TTA and BPADA monomers were respectively determined in the presence of the functional groups (respective peaks) of the aromatic tri-NH_2 (3467, 3416, 3324, and 3119 cm^{-1}/ and 1626, 1526, and 1427 cm^{-1}) and the dimethyl groups, —$C(CH_3)_2$ (3061, 2969 and 2870 cm^{-1}), C—O—C (1276 and 1225 cm^{-1}), and COO (1846 and 1771 cm^{-1}). The reaction between the TTA and BPADA to form the HPI precursor involved the destruction and formation of specific chemical bonds. The most significant peaks were observed in the reactive functional groups of —NH_2 and COOOC, each of which represented the unfunctionalized s-triazine from melamine and BPADA units that disappeared and were replaced by broad peaks in the ranges of 3700–3000 cm^{-1} and 1800 and 1600 cm^{-1} (Mittal, 2003). These peaks occurred in response to the presence of the —OH and —NH stretch mode, the carbonyl group of carboxylic acid, COOH, and the amide group, CONH. The precursor retained the main characteriztics of the backbone, which was represented as —$C(CH_3)_2$, the p-substituted benzene ring (at 1501 cm^{-1}) and C—O—C from the BPADA monomer, this suggesting that the reaction between these two species was successful without any chain cleavage.

When the TTA/BPADA HPI precursor was heated, the formation of imide rings was observed from the absorption bands that appeared at 1776 and 720 cm^{-1}. The characteriztics of the imidized peaks were presented through the absorption bands between 1780 cm^{-1} and 1724 cm^{-1} (unsymmetrical C═O of imide and symmetrical C═O of imide stretches), 1374 (C—N of imide stretch), 1102 cm^{-1} and 747 cm^{-1} (imide ring deformation) and 723 (C—N—C of imide ring formation), together with strong absorption bands around 1100–1300 cm^{-1} due to

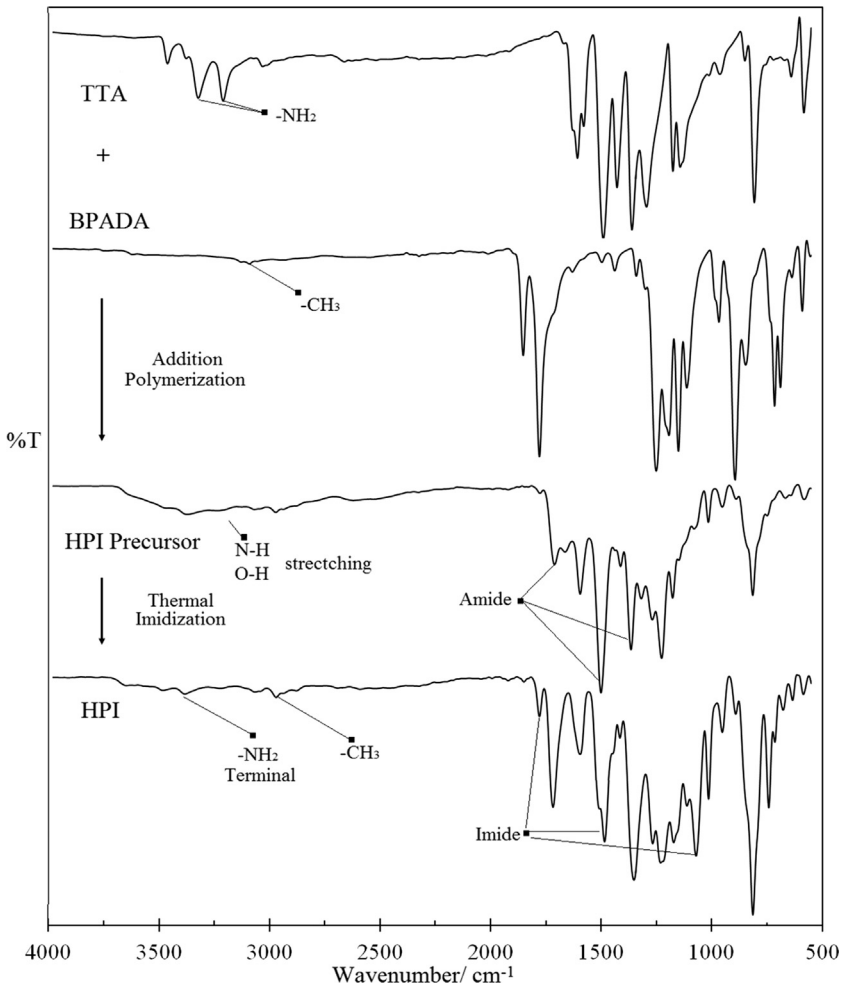

Figure 4 FT-IR spectra of the formation of TTA/BPADA HPI precursor through addition polymerization and the formation of TTA/BPADA HPI through thermal imidization.

the C—O stretching (Niyogi et al., 2001). The disappearance of the amide and carboxyl bands in the region between 3400 and 2900 cm^{-1} indicated the conversion of the TTA/BPADA HPI precursor into PI. However, this conversion was dependent on the temperature and the time. As the curing temperature was increased, the absorption at the position of 1776–720 cm^{-1} increased gradually, indicating an increasingly higher degree of imidization (Fig. 5). The dependence of the degree of imidization of the TTA/BPADA HPI precursor at various temperatures is shown in Fig. 6.

Further, the effect of temperature on the imidization process was investigated based on the fact that the absorption intensities are the same in the precursors as well as in all the cured products which are imidized at different temperatures. The bands around 1500 cm^{-1} and 720 cm^{-1} were chosen qualitatively and quantitatively because of the reproducibility of the precursor. The degree of imidization (DI) of the sample heated at a certain temperature was calculated using Eq. (1).

$$\text{Degree of Imidization} = \frac{\sum \text{imidized groups}}{\sum \text{imidizable group}} \times 100\% \qquad (1)$$

From Figs. 5 and 6, it is interesting to note that the TTA/BPADA HPI precursor was able to be imidized at >40% at a relatively low temperature (100 °C). In comparison to the imidization of unfunctionalized s-triazine (Melamine/BPADA) in a previous work (>30% at 100 °C) (Othman et al., 2015c), it is suggested that the thermal imidization of TTA/BPADA HPI appears to be more feasible at the initial stage. Furthermore, when the temperature was increased from 100 °C to 240 °C, the absorption at 1776 and 720 increased rather than decreased, this inferring that the formation of the imide ring from the TTA/BPADA HPI precursor was not reversible at high temperatures. When the degree of imidization was >90%, curing occurred at 220 °C, and the degree of imidization reached 100% within 1 h after heating at 240 °C. However, when the precursor was converted to PI, the resulting HPI molecular chain became rigid and the mobility decreased, further limiting conformational changes in the chain. To ensure that the TTA/BPADA precursor was efficiently imidized to the highest degree, it was necessary to prolong the heating at a low temperature (prebaked at 90 °C).

For other separate cases, although the propagation period can be increased by extending the reaction time, and driving

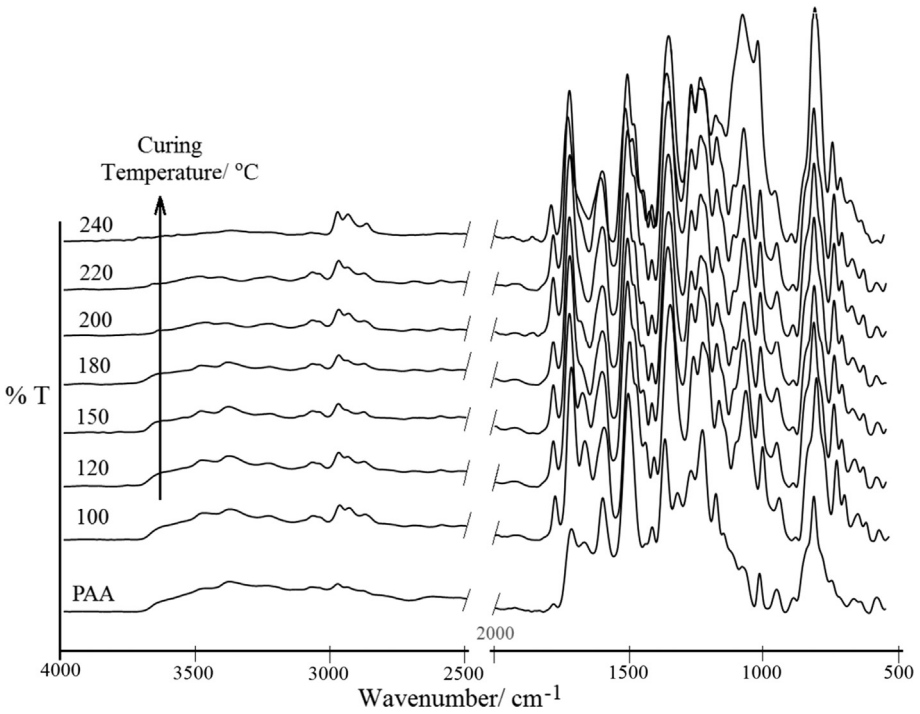

Figure 5 FT-IR of imidized products from the TTA/BPADA HPI precursor at different curing temperatures.

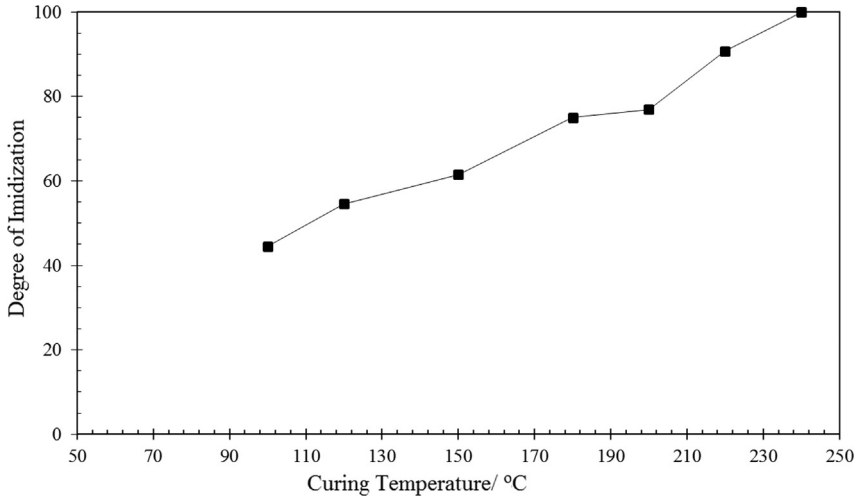

Figure 6 Dependence of degree of imidization of TTA/BPADA HPI precursor at various temperatures.

up the molecular weight, however this cannot be monitored throughout by FT-IR. No significant changes were found even when the intensities of certain peaks were increased (Fig. 7). Additionally, this did not affect the imidization of the TTA/BPADA precursor to the highest degree of polyimidization.

3.3. Chemical stability

The chemical stability and processability of the resulting TTA/BPADA HPI were studied through a solubility behavior test using various types of solvents (acidic, basic, protic and aprotic, and polar or non-polar media). In this work, the effect of the formation of premature polymers (Table 2, corresponding to molecular weight) and different curing temperatures (Table 3, corresponding to degree of imidization) on the chemical stability of TTA/BPADA HPI was studied.

From Table 2, the TTA/BPADA HPI precursor was taken out from the reaction medium at a specified time, and consequently, was thermally imidized at the same temperature. The film was tough, transparent and creasible. However, no suitable solvents were found to dissolve the TTA/BPADA HPI, and even the PI which was produced was premature (Mw = 14000 g/mol at a reaction time of 30 min). Similar results could also be seen for the TTA/BPADA HPI which had been thermally imidized, even at a low temperature (Table 3).

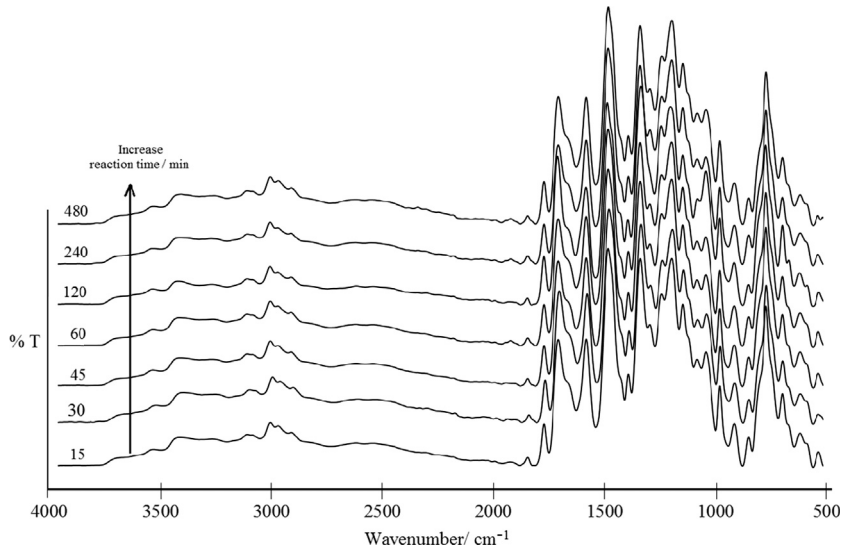

Figure 7 FT-IR of TTA/BPADA HPI precursor at different reaction times.

Table 2 Solubility of HPI series in various solvents at ambient temperature.

Solvent	Time of reaction					
	15	30	60	120	240	480
H_2SO_4[a]	– –	– –	– –	– –	– –	– –
CH_3COOH	– –	– –	– –	– –	– –	– –
KOH	– –	– –	– –	– –	– –	– –
NH_4OH	– –	– –	– –	– –	– –	– –
NMP	– –	– –	– –	– –	– –	– –
DMF	– –	– –	– –	– –	– –	– –
DMSO	– –	– –	– –	– –	– –	– –
THF	– –	– –	– –	– –	– –	– –
H_2O	– –	– –	– –	– –	– –	– –
C_2H_5OH	– –	– –	– –	– –	– –	– –
Acetone	– –	– –	– –	– –	– –	– –
Pyridine	– –	– –	– –	– –	– –	– –
CH_3Cl	– –	– –	– –	– –	– –	– –
Toluene	– –	– –	– –	– –	– –	– –
Benzene	– –	– –	– –	– –	– –	– –
Hexane	– –	– –	– –	– –	– –	– –

Key: + + Fully Soluble, + – Partial Soluble, – – Insoluble.
[a] Dissolving 0.1 g of the polymer in 10 mL solvent 1% w/V at ambient temperature.

The presence of the phenoxy substituents in the s-triazine moieties from TTA prevented the planarity. It was expected to increase in free volume and a decrease in the intermolecular interactions. However, the resulting HPIs containing s-triazine functionalized phenoxy group from TTA were found compared to unfunctionalized s-triazine from Melamine (Othman et al., 2015c). This was not surprising since functionalized s-triazine containing HPIs are necessarily planar and should be packed in highly ordered, usually crystalline, arrays. This could be one possible explanation, and also the fact that the functionalized s-triazine (Melamine/BPADA) HPI polymer was soluble.

Later, in the X-ray diffraction analysis results, the TTA/BPADA HPI showed no crystalline scattering, suggesting they exist as amorphous polymers in the solid state. Although the C—N—C in the s-triazine moieties has a planar conformation that allows close packing of dipole-alignments, the existence of longer bond lengths and angles for the former also induced a 2_1 glide-plane conformation that allowed close packing of the dipole-aligned TTA-BPADA units. This might have also restricted the polymer–solvent intermolecular interactions and hence, resulted in a weak solubility that indicated the high chemical stability of the PI. A weak solubility in organic solvents presents unique fabrication opportunities that are not available to an insoluble or less soluble PI. One such application is gas separation, where the combination of solubility and excellent mechanical and thermal properties make these polyimides good

Table 3 Solubility of HPI series in various solvents at ambient temperature.

Solvent	Degree imidization						
	0[c]	100	120	150	180	200	220
H_2SO_4[a]	−−	−−	−−	−−	−−	−−	−−
CH_3COOH	−−	−−	−−	−−	−−	−−	−−
KOH	−−	−−	−−	−−	−−	−−	−−
NH_4OH	−−	−−	−−	−−	−−	−−	−−
NMP	−−	−−	−−	−−	−−	−−	−−
DMF	−−	−−	−−	−−	−−	−−	−−
DMSO	−−	−−	−−	−−	−−	−−	−−
THF	−−	−−	−−	−−	−−	−−	−−
H_2O	−−	−−	−−	−−	−−	−−	−−
C_2H_5OH	−−	−−	−−	−−	−−	−−	−−
Acetone	−−	−−	−−	−−	−−	−−	−−
Pyridine	−−	−−	−−	−−	−−	−−	−−
CH_3Cl	−−	−−	−−	−−	−−	−−	−−
Toluene	−−	−−	−−	−−	−−	−−	−−
Benzene	−−	−−	−−	−−	−−	−−	−−
Hexane	−−	−−	−−	−−	−−	−−	−−

Key: ++ Fully Soluble, +− Soluble upon heating1, −−Insoluble.
[a] Dissolving 0.1 g of the polymer in 10 mL solvent 1% w/V at ambient temperature.

candidates for fabrication into asymmetric membranes. Gas separation studies are currently being conducted to investigate the polyimide films described in this research.

3.4. Scanning electron microscopy and electron diffraction X-ray analysis

FESEM was employed to observe the morphology of the TTA/BPADA HPI films at different curing temperatures. Fig. 8 shows that no phase separation appeared at a magnification of 30000X, which demonstrated that the TTA and BPADA monomers had reacted well. This homogeneous phase dispersion of TTA and BPADA in the TTA /BPADA HPI films was due to the contribution of similar solubility parameters, and no such microscopic or macroscopic phase was observed.

At a lower curing temperature, the hydroxyl groups that are present in the TTA/BPADA It was noted that the phase separation occurred much more easily for the cross-linking matrix during the curing procedure depending on the TTA or BPADA composition and even the type of curing agent. In this study, the focus was on the curing temperature for the imidization of the TTA/BPADA HPI precursor into HPI. The HPI precursor is usually in a crystalline state but this depends a lot on the molecular planarization HPI precursor are capable of forming intramolecular hydrogen bonds with the other precursor chains.

However, it was proven that the TTA/BPADA HPI films, which had not been fully imidized (DI < 70%: Curing temperature = 150 °C), were displayed as cavities when the lens magnification of the SEM equipment was increased. This indicated that the HPI films in this state were physically soft due to incomplete thermal imidization, and this was proven later in the micro-hardness analysis results, which will be examined in detail. These irregularities and the round-shaped cavities suddenly decreased when the HPI films were cured (Fig. 8) at a temperature 200 °C, and showed signs of brittle-fracture morphologies, where the number of round cavities suddenly disappeared (Fig. 8d) at temperatures above 200 °C. Besides that, the increase in the curing temperature was more favorable for the formation of HPI rings by the elimination of the water molecules, and the changing the constituent C, H, N and O elements, as presented by the EDX data.

The EDX data that was presented showed that there was a decrease of about 5% in the O_2 content and an increase of about 0.5% in the N_2 content. This may be attributed to the fact that during thermal imidization, a certain number of H_2O molecules will be eliminated, and the chains will be closed to form imides. The EDX data proved that increasing the temperature above 200 °C was more favorable for overcoming the steric chain structure during the imidization as less energy was required to enclose the ring. The fact is that the links were initially in a favorable steric state but were thermodynamically unstable. At elevated temperatures, the links gained enough energy to overcome their steric barriers, and underwent "link" reactions to be converted into more stable imides, as indicated by the increase in the intensities of the FTIR absorption bands that are characteriztic of the $(CO)_2NC$ imide group at higher curing temperatures. Therefore, it can be concluded that the degree of imidization increased significantly with an increase in the curing temperature. The effect of the curing temperature on the out-of-plane X-ray diffraction pattern of the TTA/BPADA HPI film is shown in Fig. 9. The diffraction patterns of the TTA/BPADA HPI films varied insignificantly with the curing temperature. The XRD result obtained also indication the TTA/BPADA HPI films are amorphous.

3.5. Hardness

The results of the Vickers hardness test for TTA-BPADA HPI at loads of 5, 500 and 1000 gmm^{-2}, and at different curing temperatures/degrees of imidisation are shown in Fig. 10.

Under the same testing conditions, the TTA-BPADA HPI data showed no ambiguity, varying from 17 to 27 $kgmm^{-2}$.

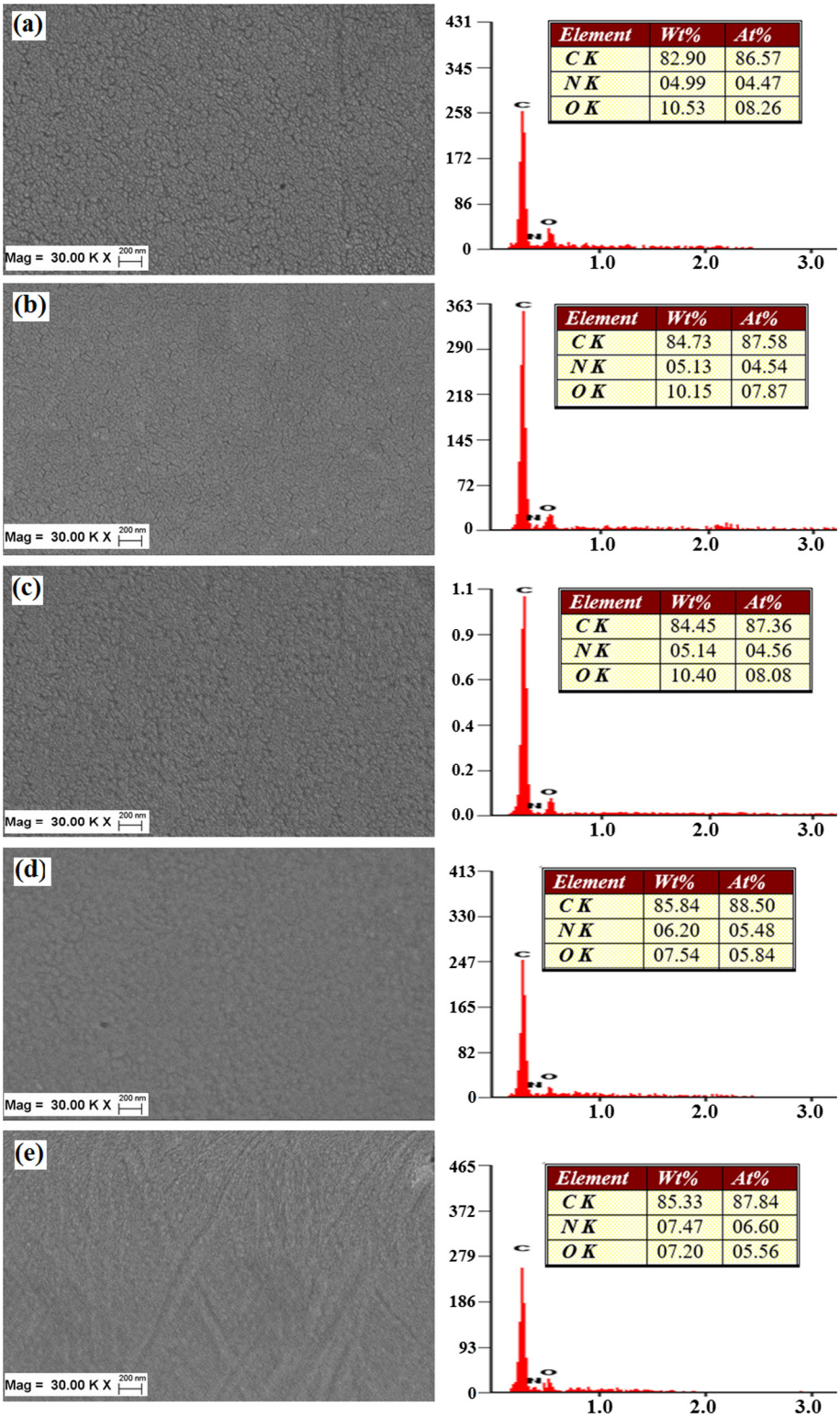

Figure 8 Use of FESEM-EDX to observe the morphology of the TTA /BPADA HPI films at different curing temperatures of (a) 100 °C, (b) 120 °C, (c) 150 °C, (d) 180 °C and (e) 220 °C.

These values indicated that the TTA-BPADA HPI system has good durability to be used in optoelectronic devices as it can withstand a mechanical force/stress/load. The durability of the TTA-BPADA HPI is mainly attributed to the rigidity of the aromatic ring in the chain backbone of the BPADA structure. However, any changes to the processing parameter (the degree of imidization, in the case of this study) will lead to changes in the micro-hardness properties. It should be noted

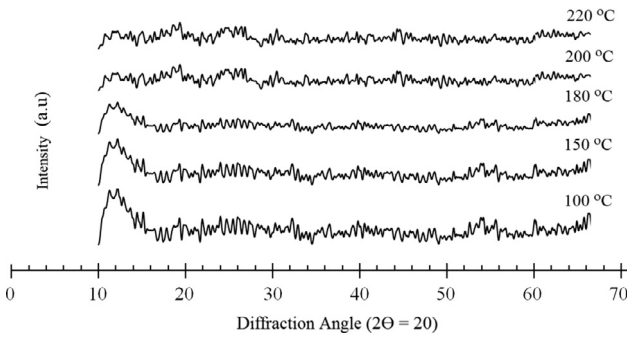

Figure 9 Effect of curing temperature on out-of-plane X-ray diffraction pattern.

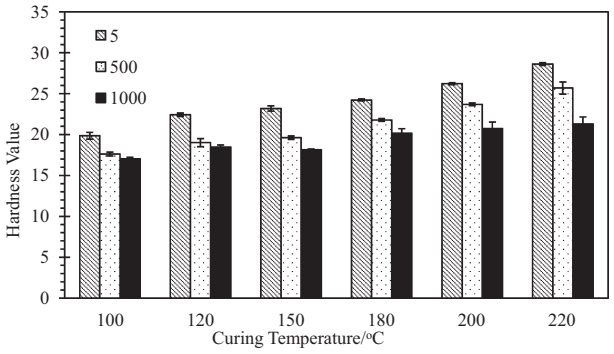

Figure 10 Average VHN values (SD) of TTA-BPADA HPI at different test loads and curing temperatures/degrees imidization.

that no effect from the indentation time was reported as the indentation time did not influence the test results, as reported by Sangwal (2000).

Fig. 10 shows a decreasing trend in the micro-hardness with an increasing indentation load. This is known as the normal indentation size effect (ISE), as reported by Sangwal (2000). Without considering variations in the indentation loads and time, the results obtained for the VHN values of the TTA-BPADA HPI in this study were in accordance with previously published values. For example, the hardness of HPIs derived from a polyamide-imide base has been reported to be in the range of 24–36 kgmm^{-2} (Ranade et al., 2002). The standard deviation of hardness in this study showed a narrow variation, similar to previous reports. This broad variation in hardness values can be due to factors such as specimen preparation, diagonal length reading error, variation in chemical chain arrangement, age, and location in the TTA-BPADA HPI films. The relationship between the average VHN values corresponding to the curing temperature/degree of imidization of the TTA-BPADA HPI film is shown in Fig. 11.

Fig. 11 shows that the VHN values of the TTA-BADA HPI films depended on the curing temperature, where the degree of imidization was dependent on the curing temperature (Fig. 6). The VHN micro-hardness values increased with increasing degrees of imidization. Typically, at low curing temperatures, the resulting TTA-BPADA HPI films had a low chain packing density as the system did not have sufficient time and energy to attain thermodynamic equilibrium during the chain alignment. Besides that, the supply of lower thermal energy induced

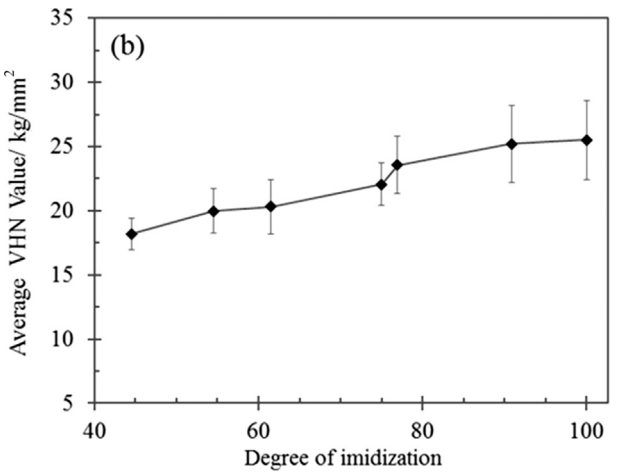

Figure 11 Relationship between the average VHN values corresponding to the degree of imidization of the TTA -BPADA HPI films.

inefficient bond vibrations around the HPI system, resulting in a lower conversion of the TTA-BPADA HPI precursor to PI. These phenomena contributed to an increase in the average chain distance (increase in free volume), which created a wider spacing between the chains. This system, which contained a high free volume, was unable to resist deformation during the indentation as the material was physically soft, and low VHN micro-hardness values were obtained.

By increasing the curing temperature, the system had sufficient time and energy to attain thermodynamic equilibrium, and the chains could be easily aligned due to the almost complete conversion of the TTA-BPADA HPI precursor to PI. These contributed to a decrease in the average chain distance and led to an increase in the chain packing density (reducing free volume). Therefore, during the indentation, the chain rotational barrier was restricted and the hardness increased, and displaying a better ability to withstand deformation. Again, the results of this study showed that the difference in the indentation load influenced the VHN values of the TTA-BPADA HPI films for the same HPI films imidized at same temperature, while a high degree of imidization improved the VHN values of the TTA-BPADA HPI films.

3.6. Thermal properties

3.6.1. TG analysis

The thermal stability of the HPI precursor in a N_2 environment is shown in Fig. 12. The TG and DTG curves show the imidization of the samples at T = 120, 150, 180, 200 and 220 °C for 1 h prior to the measurement. The TG traces revealed the minor mass loss that took place around 100 °C (indicating the removal of moisture trapped inside the HPI film) and the two stages of thermal decomposition.

The first stage of decomposition (T_1) for the PI series started at 200 °C and came to an end at about 350–400 °C. This was probably due to either the degradation of the weakest linkages or cyclodehydration. This suggestion is based on the fact that the degradation of the weakest linkage was consistent with the result reported by Chen et al. for the double-stage decomposition process for a PI system in a nitrogen atmo-

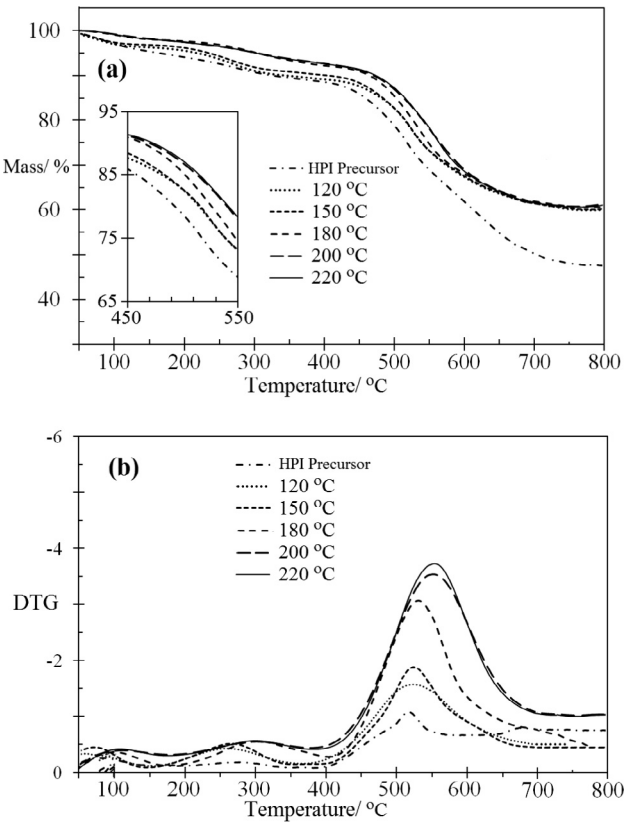

Figure 12 Effect of curing temperature on degradation temperature (a) TG curve, and (b) DTG curve.

sphere (Chen et al., 2008), which could be attributed to the weak bonds that may exist (—NH—, and —CONH—) between the side chain substituents and the degradation of the propylidene bridge C—$(CH_3)_2$ from the BPADA in the PI backbone. However, it is also believed that thermal dehydration contributed to the first stage of decomposition in HPI, as shown in Fig. 1, and this was proven by Pramoda et al. (2002) when studying the effects of the thermal imidization of the PI precursor. Fig. 12a shows that the corresponding temperature, T_1 had shifted to a higher temperature for the treated HPI compared to the HPI precursor. As the curing temperature was increased from 120 °C to 220 °C for 1 h, the T_1 almost did not appear in a thermogram because of the completion of the imidization process.

The second stage of decomposition (T_2) for the PI started around 400 °C, corresponding to the decomposition of the aromatic imide groups or heterocyclic structures (Chen et al., 2008); this is typical for aromatic polyimides in general. The analysis of the evolved gases provided a much clearer understanding of the imidization. Chen et al. (2008) and Xie and Pan (2001) reported that the major gases that are evolved during degradation are hydrocarbons, CO_2, CO, and H_2O, with hydrocarbons being evolved as the end groups during the first stage of the degradation (below 200 °C) as the side groups are broken from the main chain, while CO_2, CO, and H_2O are produced during the second stage of decomposition (ranging from 500 to 800 °C) as the main chain is broken down. However H_2O is evolved at all temperatures from around 100 °C to very high temperatures, and this indicates that at least part of the water must be an actual product of degradation and not just adventitious moisture (Xie and Pan, 2001).

This was also consistent with the work reported by Crossland et al. (1987). They believed that the CO arises directly from the imide ring, while the evolution of CO_2 may be due to (1) unreacted anhydrides; (2) amic acids, which may form either from incomplete imidization or the hydrolysis of imide rings; and (3) the decomposition of the isoimides derived from the rearrangement of the imides. The polymers investigated in this study consisted solely of carbon, hydrogen, nitrogen and oxygen elements (Fig. 8). The TG characteriztics for the thermally imidized HPI series in a nitrogen atmosphere are shown in Table 4.

There was more than 50% of residue once the degradation was completed at 800 °C, except for the TBT000 (HPI precursor). Compared to the HPI derived from Melamine /BPADA (Othman et al., 2015b,c), the TTA/BPADA HPI derivative had a 20% char residue. This high residue might have been due to the contribution of cross-linked materials, high constituents of an aromatic and imide structure. These values were consistent with the corresponding temperatures for T_{10}, T_{20} and T_1, which were shifted to higher temperatures for the treatment of the HPI precursor. This proved that increasing the temperature led to an increase in the cyclization of the amic acid group to the imide group, which relatively increased the stability of the HPI system towards degradation. Shen et al. (2013) proved that the existence of a flexible unit, such as a phenoxy-linkage, did not accelerate the degradation process. Instead, the degradation process was delayed mainly because of the combination of high temperature resistant imide units as an aromatic group in the HPI chain. Table 4 also indicates that when $T = 200$ °C, the temperature was high enough for a cyclization process, while the temperature (T_2) for a maximum rate of mass loss (ΔT_2) showed an insignificant increase in value for further increases in the curing temperature. That means the cyclization at $T = 200$ °C contributed to the decomposition stability both thermodynamically and kinetically.

3.6.2. Differential scanning calorimetry

To reveal the information about the current condition of the specimens or the processing influences of thermal history, the HPI series were further investigated by means of DSC. *Tg* characterized the segmental motion of the polymer, which was dependent on the aggregation structure of the polymer. The results are shown in Fig. 13.

Despite the fact that over 70% of all the TTA/BPADA HPI series that had been prepared was imidized, according to the FTIR results (Fig. 6) no significant endothermic peaks corresponding to the melting temperature (the crystalline region) appeared within the temperature range of 150–400 °C. This was consistently proven by the X-ray diffraction analysis results (Fig. 9), which showed that the TTA/BPADA HPI showed no crystalline scattering pattern, suggesting that it existed as an amorphous polymer in the solid state. As expected from the molecular structure, this polymer underwent a transition in the region of high temperatures exceeding 190 °C, indicating its good resistance to heat. It was apparent from a DSC scan that there was only a single distinct *Tg* in the region of 100–300 °C for each polymer and that the values changed with variations in the processing and molecular environment. Clearly, from the *Tg* in Fig. 13, the region increased

Table 4 Effect degree imidization on the thermal properties of HPI series in nitrogen atmosphere.

Sample designation	T_{10}[a]	T_{20}[a]	T_1[b]	T_2[c]	$T_{2\ on}$[d]	$T_{2\ end}$[e]	ΔT_2[f]	Char residue[g]%
TBT000	327	493	280	516	412	551	139	35.1
TBT120	405	514	260	524	450	615	165	55.0
TBT150	345	515	265	524	452	598	146	55.6
TBT180	463	526	302	531	438	605	167	57.8
TBT200	466	539	300	551	443	647	204	58.0
TBT220	473	542	301	553	440	645	205	58.0
MB11LV	–	–	–	475				34.3

[a] Temperature corresponding to percentage of mass loss, 10% and 20%.
[b] Temperature of maximum rate of mass loss; 1st stage degradation.
[c] Temperature of maximum rate of mass loss; 2st stage degradation.
[d] Onset temperature of degradation.
[e] Endset temperature of degradation.
[f] $\Delta T = T_{end} - T_{onset}$.
[g] wt% residue at 800 °C.

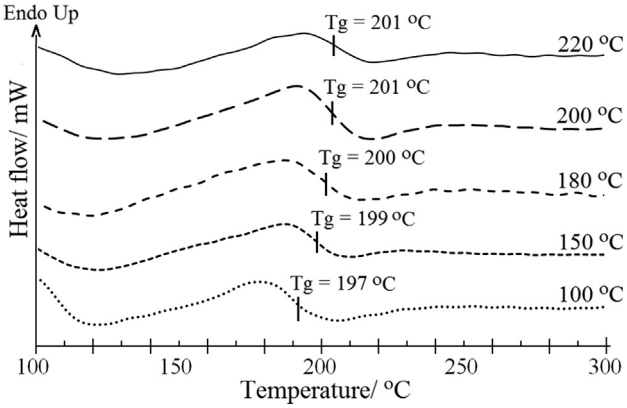

Figure 13 DSC thermogram in N_2 atmosphere corresponding to the curing temperature.

from 197 to 202 °C, which increased the curing service temperature. Again, this increasing trend in the *Tg* was due to the increasing cyclization in the HPI derivatives, which improved the thermal stability of the HPI structure. Compared to the Melamine/BPADA HPI derivative (Othman et al., 2015c), the *Tg* of the TTA/BPADA HPI was ~10 °C higher. Although the phenoxy-linkage that was functionalized in the s-triazine moieties was expected to reduce the *Tg*, due to the imparting of flexibility to the unit, it did not occur. Therefore, the reason for the increase in the *Tg* was due to the increasing rigidity of the aromatic constituent in the HPI system. However, the *Tg* in this work was close to the commercial polyimide, Ultem 1000 (*Tg*, 217 °C), based on the bisphenol-A diphthalic anhydride and m-phenylene diamine.

3.6.3. Thermal conductivity

As good candidates for thermal insulation, polymers from the PI class typically have an intrinsic thermal conductivity that is much lower than that of other polymer classes, which have the ability to resist the flow of heat. Further enhancement of this insulating capacity can be achieved by playing with many factors, such as the chemical constituents, bond strength, structure type, side group molecular weight, molecular density distribution, type and strength of defects or structural faults, size of intermediate range order, processing conditions and temperature. The thermal conductivity was strongly affected by the crystallinity (a higher crystallinity means a higher thermal conductivity). However, the XRD results (Fig. 9) indicated that the synthesised TTA/BPADA HPI was fully amorphous. Therefore, the heat conductivity of the TTA/BPADA HPI was not due mainly to the lattice vibrations (phonon). That means the mean free path of the phonon was not increased significantly at higher temperatures, and was approximately constant at low temperatures just like the heat capacity. The experimental data on the thermal conductivities and specific heat of the TTA-BPADA HPI plotted against the curing temperature are shown in Fig. 14. Both thermal conductivities and specific heat was obtained through hot disk thermal constant Analyser equipment.

In this study, the thermal conductivity of the TTA-BPADA HPI was found to be as low as 0.1070 W/mK and as high as 0.1222 W/mK. The thermal conductivity was expected to be dependent on the processing temperature. Typically, at a low curing temperature, the resulting TTA-BPADA HPI film had a low chain packing density as the system did not have sufficient time and energy to attain thermodynamic equilibrium during the chain alignment, and resulting in less of the TTA-BPADA HPI precursor being converted to PI. Since the bond strength of the TTA-BPADA HPI precursor was less than that of the TTA-BPADA HPI, the resulting TTA-BPADA HPI films had a low molecular density distribution. Therefore, the intrinsic heat transfer across the material occurred at a lower rate due to the strength of the defects or the structural faults. However, by increasing the curing temperature, the system had sufficient time and energy to attain thermodynamic equilibrium and the chains were easily aligned as the TTA-BPADA HPI precursor was mostly converted to PI, and attaining a high degree of imidization. These contributed to a decrease in the average chain distance and led to an increase in the chain packing density (reducing free volume). Therefore, the intrinsic heat transfer across the material increased due to improvements in the strength of the defects or the structural faults.

According to Fig. 14b, the thermal conductivity and specific heat of the TTA-BPADA HPI attained thermodynamic equilibrium at a 100% degree of imidization (curing temperature $\geqslant$220 °C). Although, the high degree of imidization con-

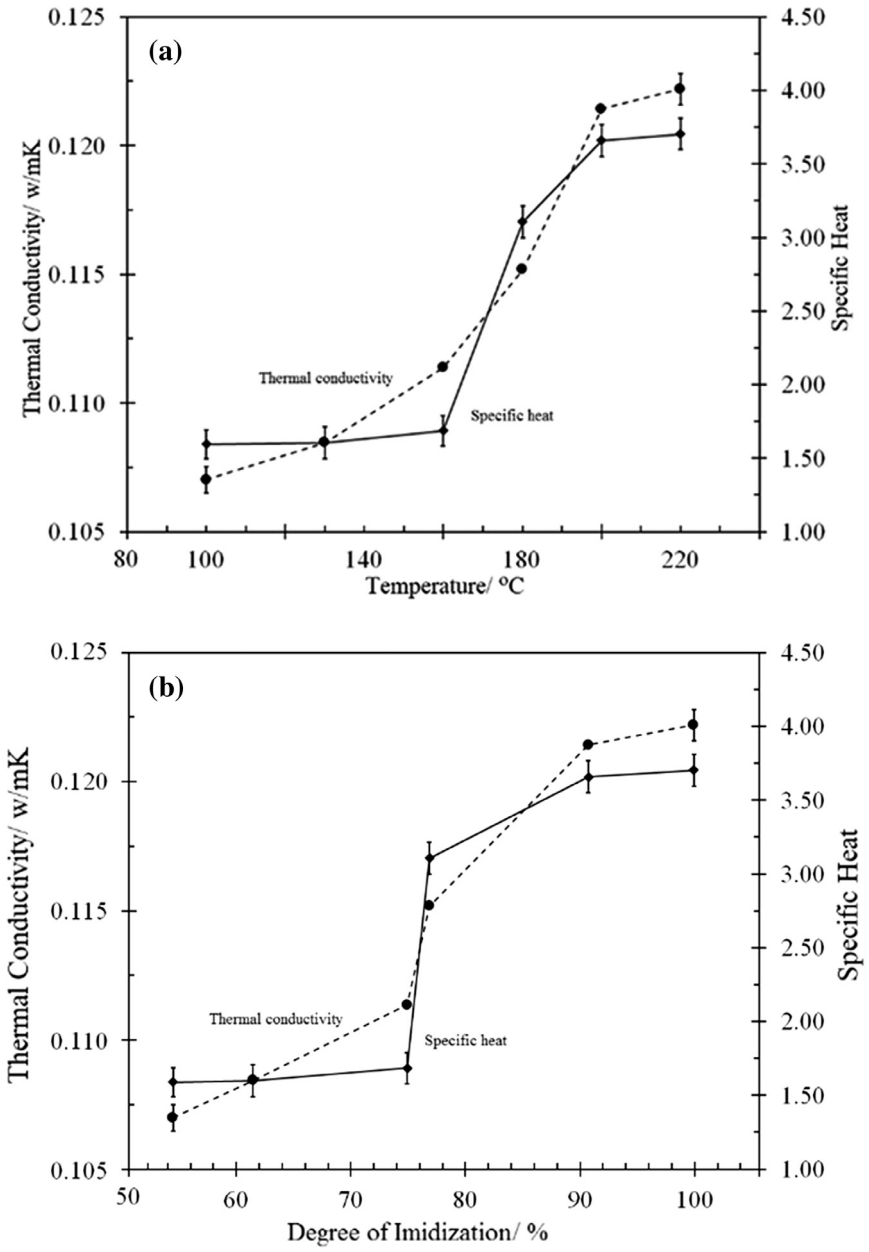

Figure 14 Experimental data of thermal conductivities and specific heat of the TTA-BPADA HPI plotted against the degree of imidization.

tributed to the high thermal conductivity of the TTA-BPADA HPI, the experimental data showed that its value was still low compared to the commercial PI 0.22 at 25 °C (Khandelwal and Mench, 2006), besides having acceptable VHN values. It was evident that the TTA-BPADA HPI showed an enhancement in its insulating quality based on the value obtained in this study.

4. Conclusion

4,4′,4″-((1,3,5-Triazine-2,4,6-triyl)tris(oxy))trianilin/4,4′-(4,4′-Isopropylidene-diphenoxy)bis(phthalic anhydride) TTA/BPADA HPI was successfully synthesized using direct nucleophilic addition between the —COOOC— groups of dianhydride and $-NH_2$ of a trianiline in Dimethylformamide (DMF) solvent. The synthesized HPIs required an optimum reaction time of about 2 h and above to yield a high molecular weight and narrow molecular weight distribution. The typical ^{1}H-NMR spectra of the HPI system consistently showed characteriztics of aromatic TTA and BPADA as the HPI backbone. The FT-IR spectra showed that the degree of imidization of the HPI series was dependent on the temperature and was completely imidized, with the degree of imidization being >80% at 200 °C. The synthesised TTA-BPADA HPI showed good chemical stability due to it insolubility in an organic solvent. The SEM morphology analysis showed that the TTA and BPADA were miscible and no phase separation was observed. The EDX data showed a decreasing O_2 content of about 5% and an increasing N_2 content of about 0.5% as the DI increased, and this may be attributed to the

fact that the amount of H_2O molecules would have been eliminated during thermal imidization, while the XRD diffraction pattern revealed that the TTA-BPADA HPI films were in the amorphous phase. The difference in the indentation load influenced the VHN values of the TTA-BPADA HPI films, while the high degree of imidization improved the VHN values of the TTA-BPADA HPI films.

The thermal stability of the TTA-BPADA HPI films was greatly improved in the fully imidized form. As for the temperature value, at 10% mass loss, the *Tg* was over 460 °C when the HPI film was fully imidized. It was found that the thermal conductivity and specific heat of the TTA-BPADA HPI attained thermodynamic equilibrium at a 90% degree of imidization (curing temperature $\geqslant$220 °C was 0.1222 W/mK). The incorporation of the s-triazine moieties in an HPI system could result in the enhancement of the thermo-chemical properties due to the existence of the HPI structure. Therefore, it is believed that this incorporated HPI structure containing s-triazine moieties in a polyimide system appears promising as a new high performance and highly functional material.

Acknowledgement

The authors wish to acknowledge the Universiti Sains Malaysia – Malaysia for sponsoring this project under PRGS-1001/PBAHAN/8046027 and RU-1001/PKIMIA/811221 research grants.

References

Ando, S., 2004. Optical properties of fluorinated polyimides and their applications to optical components and waveguide circuits. J. Photopolym. Sci. Tech. 17 (2), 219–232.

Chen, C., Huang, X., Qin, W., 2008. Preparation, characterization and thermal decomposition of polyimides with main chain containing cycloaliphatic units. J. Macromol. Sci. B 47 (1), 109–116.

Choi, M.C., Wakita, J., Ha, C.S., Ando, S., 2009. Highly transparent and refractive polyimides with controlled molecular structure by chlorine side groups. Macromole 42 (14), 5112–5120.

Cornelius, C., Marand, E., 2002. Hybrid silica-polyimide composite membranes: gas transport properties. J. Membr. Sci. 202 (1–2), 97–118.

Crossland, B., Knight, G.J., Wright, W.W., 1987. Thermal degradation of some polyimides. Polym. Int. 19 (3–4), 291–301.

Dallas, P., Bourlinos, A.B., Petridis, D., Boukos, N., Papadokostaki, K., Niarchos, D., Guskos, N., 2008. Synthesis and characterization of 2-D and 3-D covalent networks derived from triazine central cores and bridging aromatic diamines. Polym 49 (5), 1137–1144.

Harris, F., 1990. Polyimides. Chapman and Hall New York, New York.

Jabbari, E., Nozari, S., 1999. Synthesis of acrylic acid hydrogel by gamma-irradiation cross-linking of polyacrylic acid in aqueous solution. Iran. Polym. J. 8 (4), 263–270.

Khandelwal, M., Mench, M.M., 2006. Direct measurement of through-plane thermal conductivity and contact resistance in fuel cell materials. J. Power Source 161 (2), 1106–1115.

Mahapatra, S.S., Karak, N., 2007. Hyperbranched aromatic polyamines with s-triazine rings. J. Appl. Polym. Sci. 106 (1), 95–102.

Mittal, K., 1984. Polyimides: Synthesis, Characterization, and Applications, vol. 1 & 2 (vol. 1). Plenum Press, New York.

Mittal, K., 2003. Polyimides and Other High Temperature Polymers: Synth, Charac and Appl. VSP.

Mittal, K.L., 2007. Polyimides and Other High Temperature Polymers: Synthesis, Characterization, and Applications. VSP.

Mittal, K., 2009. Polyimides and Other High Temperature Polymers: Synthesis, Characterization, and Applications. Brill Academic Pub..

Niyogi, S., Maiti, S., Adhikari, B., 2001. Cyclodehydration of poly (amic acid) to polyimide. Int. J. Polym. Mater. 49 (3), 323–330.

Othman, M.B.H., Ming, N.A.S., Akil, H.M., Ahmad, Z., 2011. Dependence of the dielectric constant on the fluorine content and porosity of polyimides. J. Appl. Polym. Sci. 121 (6), 3192–3200.

Othman, M.B.H., Ahmad, Z., Akil, H.M., Zakaria, M.R., Ullah, F., 2015a. The effects of the Si—O—Si segment presence in BAPP/BPDA polyimide system on morphology and hardness properties for opto-electronic application. Mater. Design 82, 98–105.

Othman, M.B.H., Ahmad, Z., Osman, H., Omar, M.F., Akil, H.M., 2015b. Thermal degradation behavior of a flame retardant melamine derivative hyperbranched polyimide with different terminal groups. RSC Adv. 5 (112), 92664–92676.

Othman, M.B.H., Akil, H.M., Osman, H., Khan, A., Ahmad, Z., 2015c. Synthesis, characterisation and thermal properties of hyperbranched polyimide derived from melamine via emulsion polymerisation. J. Therm. Anal. Calorim. 120 (3), 1–14.

Pramoda, K.P., Liu, S., Chung, T.-S., 2002. Thermal imidization of the precursor of a liquid crystalline polyimide. Macromol. Mater. Eng. 287 (12), 931–937.

Ranade, A., D'Souza, N.A., Gnade, B., 2002. Exfoliated and intercalated polyamide-imide nanocomposites with montmorillonite. Polym 43 (13), 3759–3766.

Sangwal, K., 2000. On the reverse indentation size effect and microhardness measurement of solids. Mater. Chem. Phys. 63 (2), 145–152.

Shen, J., Zhang, Y., Chen, W., Wang, W., Xu, Z., Yeung, K.W., Yi, C., 2013. Synthesis and properties of hyperbranched polyimides derived from novel triamine with prolonged chain segments. J. Polym. Sci. Part A: Polym. Chem. 51 (11), 2425–2437.

Sojitra, P.N., Patel, K.C., Patel, H.S., 2010. High performance polyamides based on s-triazine ring: synthesis and characterization. High Perform. Polym. 22 (8), 974–988.

Sroog, C.E., 1976. Polyimides. J. Polym. Sci.: Macromol. Rev. 11 (1), 161–208.

Suzuki, T., Yamada, Y., Tsujita, Y., 2004. Gas transport properties of 6FDA-TAPOB hyperbranched polyimide membrane. Polym 45 (21), 7167–7171.

Xie, W., Pan, W.P., 2001. Thermal characterization of materials using evolved gas analysis. J. Therm. Anal. Calorim. 65 (3), 669–685.

Zhang, F., Srinivasan, M., 2007. Multilayered gold-nanoparticle/polyimide composite thin film through layer-by-layer assembly. Langmuir 23 (20), 10102–10108.